Maximum cumulant method for studying condensation-evaporation phase transitions

G. J. dos Santos,[*] D. H. Linares,[†] and A. J. Ramirez-Pastor[‡]
Departamento de Física, Instituto de Física Aplicada, Universidad Nacional de San Luis-CONICET, Ejército de Los Andes 950, D5700HHW, San Luis, Argentina

(Received 23 March 2018; revised manuscript received 31 July 2018; published 25 September 2018)

In a previous paper [G. J. dos Santos, D. H. Linares, and A. J. Ramirez-Pastor, J. Stat. Mech. (2017) 073211] a methodology for the determination of the critical point of the condensation phase transition occurring in monolayers of linear adsorbates (k-mers) was presented. The maximum cumulant method was developed from the phenomenological observation that the fourth-order Binder cumulant and the isotherm inflection point are produced at the same value of chemical potential. In the present work, mathematical arguments are presented to show analytically that the previously mentioned relationship is satisfied by evaporation-condensation systems under the conditions that: (i) the surface coverage distribution function is a bimodal distribution composed of a linear combination of two normalized functions $g_1(\theta)$ and $g_2(\theta)$ with zero overlap and mean values θ_1 and θ_2, respectively; and (ii) $g_1(\theta)$ and $g_2(\theta)$ are unimodal distributions that are symmetric with respect to the middle point $(\theta_1+\theta_2)/2$. In addition, numerical results from Monte Carlo simulations of four different adsorption-desorption systems (linear k-mers on square and triangular lattices, S-shaped k-mers on square lattices and k^2-mers on square lattices) are presented to check the theoretical results and to provide evidence of the general validity and robustness of the method.

DOI: 10.1103/PhysRevE.98.032134

I. INTRODUCTION

The two-dimensional lattice-gas model with nearest-neighbor interactions has been extensively explored in recent decades. This is due in part to the fact that this system is known to provide a useful model for studies of phase transitions occurring in many adsorbed monolayer films [1–5]. Among the common types of phase transitions are condensation of gases, melting of solids, transitions from paramagnet to ferromagnet, order-disorder transitions, and so on.

From a theoretical point of view, an extra term in the partition function is required when nearest-neighbor interactions are present. With this extra term, only partition functions for the whole system can be written. Ising [6] gave an exact solution to the one-dimensional lattice problem in 1925. All other cases are expressed in terms of series solution [7–9], except for the special case of two-dimensional lattices at half-coverage, which was exactly solved by Onsager [10] in 1944.

The problem is even more complex for adsorbates occupying more than one surface site. In fact, most adsorbates involved in adsorption experiments are polyatomic in the sense that, when adsorbed, their typical size is larger than the distance between the nearest-neighbor local minima of the gas-solid potential. Examples of this kind of system are monolayer films of n-alkanes adsorbed on monocrystalline surfaces of metals, such as Pt(111) [11] and Au(111) [12,13]. Even the simplest nonspherical molecules such as N_2 and O_2 may adsorb on more than one site depending on the surface structure [14–19]. This effect, so-called multisite occupancy adsorption, introduces a high degree of local correlation in the adsorption theories. Consequently, it has been difficult to formulate, analytically, the statistics of occupation for interacting polyatomics or k-mers (particles occupying several k contiguous lattice sites).

One way of overcoming these drawbacks complications is to use the Monte Carlo (MC) simulation method [20–39]. MC technique is a valuable tool for studying surface molecular processes, which has been extensively used to simulate many surface phenomena including phase transitions [20–35], adsorption [36–38], diffusion [39], among others.

In this line of work, an alternative methodology based on a combination of the histogram reweighting (HR) technique [40–42] and on the fourth-order Binder cumulant [43] was developed in a recent article from our research group [44]. The technique, called "maximum cumulant method" (MCM), was tested in a system of interacting monomers in which the critical point can be determined exactly. Once the validity and the accuracy of the methodology was established, MCM was applied to the study of the phase transition occurring in a system of attractive dimers adsorbed on 2D square lattices. The method proved to be a very useful tool for the research of phase transitions in lattice-gas models.

More recently, MCM was applied to the study of the phase behavior of attractive k-mers adsorbed on square lattices in the presence of anisotropy [45]. To simulate the effect of the anisotropy, the k-mers were deposited along one of the directions of the lattice forming a nematic phase. The methodology was used to calculate the critical point of the condensation transition occurring in the system. The results, obtained for k ranging from 2 to 7, showed that: (i) the transition coverage

[*]gjdossantos@unsl.edu.ar
[†]Corresponding author: dlinares@unsl.edu.ar
[‡]antorami@unsl.edu.ar

exhibits a decreasing behavior when it is plotted as a function of the k-mer size; and (ii) the transition temperature, T_c, exhibits a power-law dependence on k, $T_c \sim k^{0.4}$, shifting to higher values as k increases. The simulation data were validated by comparing with mean-field analytical results.

In Refs. [44,45], the calculations were developed based on a fundamental assumption: for condensation-evaporation phase transitions, the maximum of the Binder cumulant as a function of the chemical potential and the inflection point of the adsorption isotherm (surface coverage as a function of the chemical potential) take place at the same value of chemical potential (μ_*). Even though this condition was confirmed in several adsorption systems (monomers, isotropic dimers, linear and bent trimers, linear and tortuous tetramers, and anisotropic phases of aligned k-mers), it has not been demonstrated yet by analytical methods. The objective of this work is to provide a thorough study in this direction. For this purpose, the surface coverage distribution function has been modelled as a bimodal distribution composed of a linear combination of two normalized functions. The robustness of the formulation was corroborated (1) by extending the results to the thermodynamic limit, where the surface coverage distribution function is a bimodal distribution composed of two Dirac delta functions; and (2) studying, via MC simulations, linear k-mers on square and triangular lattices, S-shaped k-mers on square lattices, and k^2-mers on square lattices.

The paper is organized as follows. The theoretical basis of the MCM for studying condensation-evaporation phase transitions is presented in Sec. II. Details of the MC simulations and the corresponding results for four different adsorption systems (linear k-mers on square and triangular lattices, S-shaped k-mers on square lattices, and k^2-mers on square lattices) are given in Sec. III. Finally, the general conclusions are drawn in Sec. IV.

II. THEORY: MAXIMUM CUMULANT METHOD FOR STUDYING CONDENSATION-EVAPORATION PHASE TRANSITIONS

In this section we will show that for condensation-evaporation systems the maximum of the Binder cumulant and the isotherm inflection point take place at the same value of the chemical potential ($\mu*$).

A. Finite systems

From the two-state approximation [46], it is well known that the condition for the two phases coexistence, $\mu_{\text{liquid}} = \mu_{\text{vapor}}$, is automatically satisfied when the areas under the two peaks of the density distribution function are the same. In addition, for finite size systems, the value of chemical potential at which the inflection point is found, is the same value that produces a density distribution with equal areas under the peaks [44].

Taking into account the expected behavior of these systems and the simulation results obtained in previous works [44] regarding the surface coverage distribution function, (see Fig. 1), we will consider in this development a distribution function $f(\theta)$ with the following features ($\theta = kN/M$ is the lattice coverage, N is the number of particles and M is the total number of lattice sites). This $f(\theta)$ is a bimodal distribution composed of a linear combination of two normalized functions $g_1(\theta)$ and $g_2(\theta)$ with mean values θ_1 and θ_2 respectively, with zero overlap. In addition, $g_1(\theta)$ and $g_2(\theta)$ are unimodal distributions that are symmetric with respect to the middle point $(\theta_1 + \theta_2)/2$. In this way, $g_1(\theta)$ and $g_2(\theta)$ accounts for the density distribution functions of the vapor and liquid phases, respectively. Therefore, $f(\theta)$ can be expressed as

$$f(\theta) = P\, g_1(\theta) + (1 - P)\, g_2(\theta), \tag{1}$$

where P ($P \in [0, 1]$) and $(1 - P)$ are the weights of the vapor and liquid distributions, respectively (see Fig. 2). It is clear

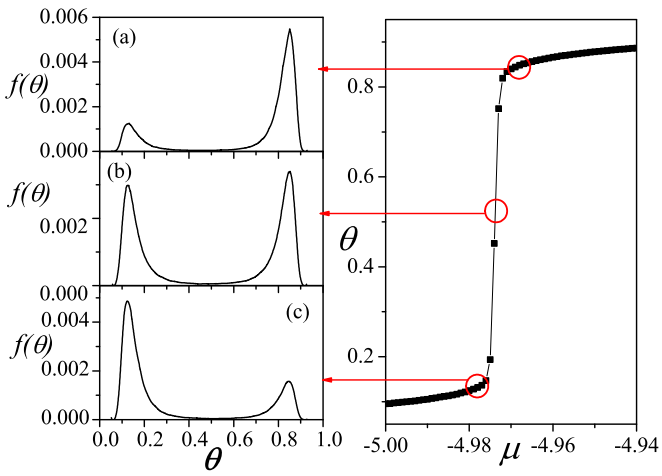

FIG. 1. Typical behavior of the surface coverage distribution function for a condensation-evaporation system. The curves were obtained from MC calculations of a system of attracting dimers adsorbed on a square lattice. The isotherm helps to visualize the state of the system corresponding to each configuration of the distribution function.

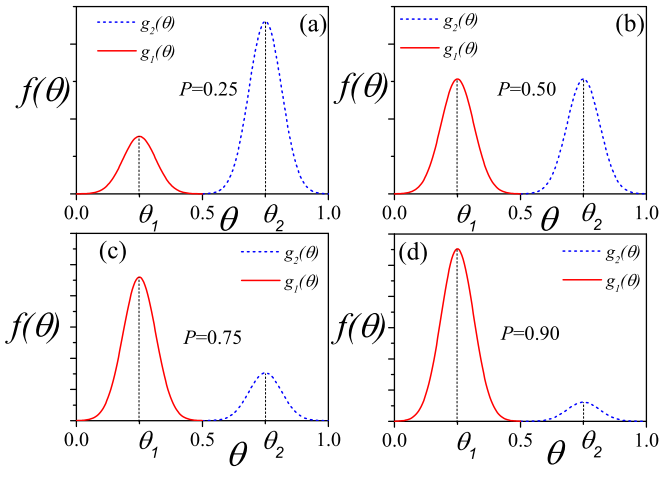

FIG. 2. Schematic representation of the construction of the surface coverage distribution function $f(\theta)$ for different values of P: (a) $P = 0.25$; (b) $P = 0.50$; (c) $P = 0.75$; and (d) $P = 0.90$. The figures show the two unimodal component distribution functions $g_1(\theta)$ (solid red line) and $g_2(\theta)$ (dashed blue line) along with their corresponding mean values, θ_1 and θ_2, respectively.

that, if we work at constant temperature (isotherms), as is the case of this study, the parameter P is a monotonically decreasing function of the chemical potential μ. At this point, it is necessary to clarify that $f(\theta)$ represents the distribution of a finite-size system with characteristic length L. In the thermodynamic limit ($L \to \infty$) $g_1(\theta)$ and $g_2(\theta)$ approx to two Dirac δ. From the arguments presented above and taken into account the way that $f(\theta)$ was defined, it is clear that the inflection point of the isotherm takes place when $P = 0.5$. In this way, to show that the Binder cumulant has a maximum at $P = 0.5$ is equivalent to show that its maximum and the inflection point of the isotherm take place at the same value of μ. As follows, we will proceed with this task.

The fourth-order Binder cumulant is defined as

$$U_L = 1 - \frac{\langle m^4 \rangle}{3\langle m^2 \rangle^2}, \tag{2}$$

where $\langle ... \rangle$ is used to indicate the average value and m is the order parameter defined as usual for a condensation-evaporation system,

$$m = \theta - \langle \theta \rangle. \tag{3}$$

The Binder cumulant has a maximum when $\frac{\langle m^4 \rangle}{3\langle m^2 \rangle^2}$ has a minimum. We are going to analyze the numerator and denominator of this fraction separately. We will begin with $\langle m^2 \rangle$.

Given that $m = \theta - \langle \theta \rangle$, then

$$\langle m^2 \rangle = \langle \theta^2 \rangle - \langle \theta \rangle^2. \tag{4}$$

It is necessary to calculate the following mean values $\langle \theta^2 \rangle$ and $\langle \theta \rangle$:

$$\langle \theta \rangle = \int_0^1 \theta f(\theta) d\theta, \tag{5}$$

$$\langle \theta \rangle = P \int_0^1 \theta g_1(\theta) d\theta + (1 - P) \int_0^1 \theta g_2(\theta) d\theta. \tag{6}$$

Given that θ_1 and θ_2 are the mean values of $g_1(\theta)$ and $g_2(\theta)$, respectively, we have that

$$\langle \theta \rangle = P\theta_1 + (1 - P)\theta_2. \tag{7}$$

Calculating $\langle \theta^2 \rangle$ in a similar way,

$$\langle \theta^2 \rangle = \int_0^1 \theta^2 f(\theta) d\theta, \tag{8}$$

$$\langle \theta^2 \rangle = P \int_0^1 \theta^2 g_1(\theta) d\theta + (1 - P) \int_0^1 \theta^2 g_2(\theta) d\theta. \tag{9}$$

We obtain

$$\langle \theta^2 \rangle = P\left[\sigma_1^2 + \theta_1^2\right] + (1 - P)\left[\sigma_2^2 + \theta_2^2\right]. \tag{10}$$

where σ_1^2 and σ_2^2 represents the variances of the distributions $g_1(\theta)$ and $g_2(\theta)$, respectively.

Then,

$$\langle m^2 \rangle = \langle \theta^2 \rangle - \langle \theta \rangle^2, \tag{11}$$

$$\langle m^2 \rangle = P\left[\sigma_1^2 + \theta_1^2\right] + (1 - P)\left[\sigma_2^2 + \theta_2^2\right] - [P\theta_1 + (1 - P)\theta_2]^2. \tag{12}$$

The most direct way to show that the fraction $\frac{\langle m^4 \rangle}{3\langle m^2 \rangle^2}$ has a minimum at $P = 0.5$ is to show that $\langle m^2 \rangle$ has a maximum and $\langle m^4 \rangle$ has a minimum simultaneously at $P = 0.5$. To find if $\langle m^2 \rangle$ has a maximum and its location, we need to find the values of P for which its derivative ($\frac{d\langle m^2 \rangle}{dP}$) is equal to zero. Therefore, we need to find an expression for the derivative of $\langle m^2 \rangle$ with respect to P,

$$\frac{d\langle m^2 \rangle}{dP} = \sigma_1^2 + \theta_1^2 - \sigma_2^2 - \theta_2^2 - 2[P\theta_1 + (1 - P)\theta_2](\theta_1 - \theta_2). \tag{13}$$

Given the symmetry relation between $g_1(\theta)$ and $g_2(\theta)$, it follows that $\sigma_1^2 = \sigma_2^2$. Therefore, it is straightforward to show that Eq. (13) vanishes for $P = 0.5$, and studying the behavior of its second derivative,

$$\frac{d^2\langle m^2 \rangle}{dP^2} = -2(\theta_1 - \theta_2)(\theta_1 - \theta_2), \tag{14}$$

$$\frac{d^2\langle m^2 \rangle}{dP^2} = -2(\theta_1 - \theta_2)^2, \tag{15}$$

$$\frac{d^2\langle m^2 \rangle}{dP^2} < 0, \tag{16}$$

we can conclude that $\langle m^2 \rangle$ has a maximum at $P = 0.5$.

Now we turn our attention to the numerator of the fraction $\frac{\langle m^4 \rangle}{3\langle m^2 \rangle^2}$, $\langle m^4 \rangle$. Given that $m = \theta - \langle \theta \rangle$, we have

$$\langle m^4 \rangle = \langle \theta^4 \rangle - 4\langle \theta^3 \rangle \langle \theta \rangle + 6\langle \theta^2 \rangle \langle \theta \rangle^2 - 3\langle \theta \rangle^4. \tag{17}$$

At next, the mean values $\langle \theta^3 \rangle$ and $\langle \theta^4 \rangle$ are calculated in the same way that we obtained $\langle \theta \rangle$ and $\langle \theta^2 \rangle$ previously. Beginning with $\langle \theta^3 \rangle$, we have

$$\langle \theta^3 \rangle = \int_0^1 \theta^3 f(\theta) d\theta, \tag{18}$$

$$\langle \theta^3 \rangle = P \int_0^1 \theta^3 g_1(\theta) d\theta + (1 - P) \int_0^1 \theta^3 g_2(\theta) d\theta. \tag{19}$$

Repeating the procedure adopted earlier, we obtain

$$\langle \theta^3 \rangle = P\left[\mu_{31} + 3\sigma_1^2\theta_1 + \theta_1^3\right] + (1 - P)\left[\mu_{32} + 3\sigma_2^2\theta_2 + \theta_2^3\right], \tag{20}$$

where μ_{31} and μ_{32} are the third central moments of the distributions $g_1(\theta)$ and $g_2(\theta)$, respectively.

At next we calculate $\langle \theta^4 \rangle$

$$\langle \theta^4 \rangle = \int_0^1 \theta^4 f(\theta) d\theta, \tag{21}$$

$$\langle \theta^4 \rangle = P \int_0^1 \theta^4 g_1(\theta) d\theta + (1 - P) \int_0^1 \theta^4 g_2(\theta) d\theta. \tag{22}$$

Operating, we obtain

$$\langle \theta^4 \rangle = P\left[\mu_{41} + 4\mu_{31}\theta_1 + 6\sigma_1^2\theta_1^2 + \theta_1^4\right] + (1 - P)\left[\mu_{42} + 4\mu_{32}\theta_2 + 6\sigma_2^2\theta_2^2 + \theta_2^4\right], \tag{23}$$

where μ_{41} and μ_{42} are the fourth central moments of the distributions $g_1(\theta)$ and $g_2(\theta)$, respectively.

Before substituting the expressions for $\langle\theta\rangle$, $\langle\theta^2\rangle$, $\langle\theta^3\rangle$, and $\langle\theta^4\rangle$ into Eq. (17), it is necessary to notice that $\sigma_1^2 = \sigma_2^2 = \sigma^2$ and $\mu_{41} = \mu_{42} = \mu_4$ given the relation between $g_1(\theta)$ and $g_2(\theta)$. Therefore, the final expression for $\langle m^4\rangle$ is given by

$$\langle m^4\rangle = \mu_4 - (-1+P)P[6\sigma^2 + (1+3(-1+P)P) \times (\theta_1-\theta_2)^2](\theta_1-\theta_2)^2. \quad (24)$$

To show that $\langle m^4\rangle$ has a minimum we must find the values of P for which its derivative vanishes

$$\frac{d\langle m^4\rangle}{dP} = -(-1+2P)\{6\sigma^2+[1+6(-1+P)P](\theta_1-\theta_2)^2\} \times (\theta_1-\theta_2)^2. \quad (25)$$

It can be seen from the previous equation that $\frac{d\langle m^4\rangle}{dP} = 0$ for $P = 0.5$. Finding an expression for the second derivative of $\langle m^4\rangle$ will allow us to determine if it has a maximum or a minimum at $P = 0.5$,

$$\frac{d^2\langle m^4\rangle}{dP^2} = [-12\sigma^2 + (\theta_1-\theta_2)^2](\theta_1-\theta_2)^2. \quad (26)$$

As we stated at the beginning of this section, $g_1(\theta)$ and $g_2(\theta)$ accounts for the density (or lattice coverage) distributions of the vapor and liquid phases, respectively, for a finite size system. As the size of the system increases, these distributions become narrower and more defined around θ_1 and θ_2, respectively, in such a way that at the thermodynamic limit $g_1(\theta)$ and $g_2(\theta)$ become two Dirac δ. Therefore, as $L \to \infty$, the variance $\sigma^2 \to 0$ while $(\theta_1-\theta_2)^2$ remains constant, then $-12\sigma^2 + (\theta_1-\theta_2)^2 > 0$ and

$$\frac{d^2\langle m^4\rangle}{dP^2} > 0. \quad (27)$$

Although Eq. (27) is satisfied in the thermodynamic limit, it is a sufficient condition to require that $(\theta_1-\theta_2)^2 > 12\sigma^2$. Hence, $\langle m^4\rangle$ has a minimum at $P = 0.5$.

Having found that $\langle m^2\rangle$ has a maximum and $\langle m^4\rangle$ has a minimum simultaneously at $P = 0.5$, we can confirm that the fraction $\langle m^4\rangle/3\langle m^2\rangle^2$ has a minimum at that point and therefore the fourth-order Binder cumulant has a maximum at $P = 0.5$. In this way it is demonstrated that for evaporation-condensation systems or any system whose distribution function presents the general features mentioned at the beginning of this section, the maximum of the fourth-order Binder cumulant and the inflection point of the isotherm take place at the same value of μ. Given that the hypotheses proposed for this deduction are not based on the structure of the systems, but only on the characteristics of the density distribution, we can say that the MCM is as general as the aforementioned hypotheses are. In Sec. III, we present a set of calculations made via Monte Carlo simulations for a variety of systems, to show this generality. In addition, a formulation based on the partition function, suggested by one of the referees is included in the Appendix.

B. The thermodynamic limit

As we stated in the previous section, the density distribution of a typical condensation-evaporation system in the thermodynamic limit ($L \to \infty$) is a bimodal distribution composed of two Dirac δ functions centered at θ_1 and θ_2 where θ_1 and θ_2 represents the surface coverage or density of the diluted and condensed phases, respectively. Therefore, it is important to corroborate that the properties found in the previous section regarding the maximum of the Binder cumulant and the isotherm inflection point, still holds for an infinite system. In this section, we will show that for every condensation-evaporation system in the thermodynamic limit, the maximum of the Binder cumulant and the inflection point of the isotherm always take place at the same value of chemical potential. From the above, we can represent the density distribution for an infinite system in the following form:

$$f(\theta) = P\delta(\theta-\theta_1) + (1-P)\delta(\theta-\theta_2), \quad (28)$$

where P and $(1-P)$ represent the weights of the two distributions. In the same way as in the previous section, if we can show that the cumulant has a maximum at $P = 0.5$, we will be showing that it coincides with the inflection point of the isotherm. To find an expression for the fourth-order Binder cumulant,

$$U = 1 - \frac{\langle m^4\rangle}{3\langle m^2\rangle^2}. \quad (29)$$

We need to find $\langle m^2\rangle$ and $\langle m^4\rangle$ where $m = \theta - \langle\theta\rangle$ is the order parameter. Proceeding in a similar way as we did in the previous section, the following expressions can be obtained without major difficulties,

$$\langle m^2\rangle = (\theta_2-\theta_1)^2P(1-P), \quad (30)$$

$$\langle m^4\rangle = (\theta_2-\theta_1)^4P(1-P)[1+3(P-1)P]. \quad (31)$$

Therefore, the Binder cumulant is given by

$$U = 2 + \frac{1}{3(P-1)P}, \quad (32)$$

and to find the location of its maximum we need to find the values of P for which its derivative vanishes. Taking the derivative on the last expression, we obtain

$$\frac{dU}{dP} = -\left(\frac{1}{3(P-1)P}\right)^2 3[(P-1)+P], \quad (33)$$

$$\frac{dU}{dP} = \frac{1-2P}{3(P-1)^2P^2}. \quad (34)$$

From the previous equation it is easy to see that $\frac{dU}{dP} = 0$ for $P = 0.5$. To check that it is a maximum we need to evaluate the second derivative of the Binder cumulant given by

$$\frac{d^2U}{dP^2} = \frac{2(3P^2-3P+1)}{3(P-1)^3P^3}. \quad (35)$$

It is clear that for all values of P,

$$\frac{d^2U}{dP^2} < 0, \quad (36)$$

and therefore the fourth-order Binder cumulant has a maximum at $P = 0.5$ showing that it is produced for the same value of chemical potential for which the isotherm inflection point is found.

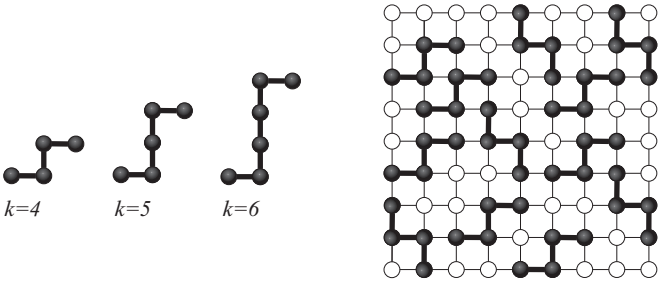

FIG. 3. Representation of tortuous S-shaped k-mers or S-mers (sometimes mentioned as zigzag adsorbates). A S-mer of size k is composed of a central linear segment of size $(k-2)$ plus two extra units attached to the ends of this segment in perpendicular direction to this and in opposite direction to each other. In the right is shown a system of S-shaped k-mers of size $k=4$ adsorbed on a square lattice.

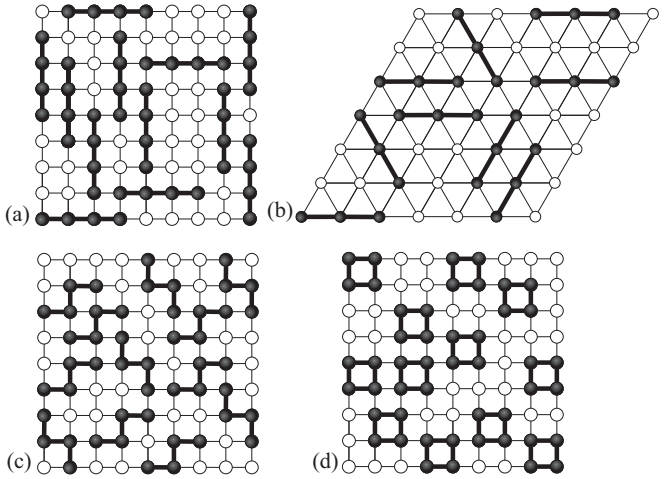

FIG. 4. Schematic representation of the different systems under study. The surface is modelled by a square or triangular array of $M = L \times L$ lattice sites with periodic boundary conditions. In part (a) is represented a system of linear k-mers ($k=4$) adsorbed on a square lattice. The system of linear trimers ($k=3$) adsorbed on a triangular lattice is shown in part (b). In the lower part of the figure are represented the systems corresponding to S-shaped k-mers of size $k=4$ adsorbed on a square lattice (c) and a system of square tiles or k^2-mers of size $k=2$ (d).

III. MODEL AND SIMULATION SCHEME

This section is devoted to verify the previous theoretical results via Monte Carlo simulations for several types of systems. At first, a linear k-mers adsorption-desorption system with attractive adsorbate-adsorbate interactions was simulated on square and triangular lattices. In addition other types of adsorbates such as square tiles of size $k \times k$ (k^2-mers) and tortuous k-mers (S-shaped k-mers) were considered.

A. Model

In this subsection, we describe the lattice-gas model for the adsorption-desorption systems mentioned above. The surfaces are represented by two different 2D lattices with periodic boundary conditions, a square and a triangular one, composed of $M = L \times L$ adsorptive sites with connectivity $c=4$ and $c=6$, respectively. We will consider three species of adsorbates:

(1) Linear k-mers: a linear molecule having k identical units, each of which occupies one lattice site. The distance between k-mer units is assumed in registry with the lattice constant.

(2) S-shaped k-mers (S-mers): a tortuous k-mer occupying k contiguous sites of the lattice forming an "S". Particularly, a S-shaped k-mer is composed of a linear segment of size $(k-2)$ with one extra monomer at each end, in perpendicular directions with respect to the main segment (see Fig. 3).

(3) Square tiles of size $k \times k$ (k^2-mers): square adsorbate occupying $k \times k$ sites when it is adsorbed.

Particularly the systems studied were: linear k-mers on square lattices, linear k-mers on triangular lattices, S-shaped k-mers on square lattices and k^2-mers on square lattices as it can be seen in Fig. 4. In all cases, lateral attractive interactions were considered between nearest-neighbor adsorbed particles. In addition, the bond energy between the units belonging to the same adsorbate is larger than the adsorption energy per unit and the lateral interaction energy. In this way, the particles can adsorb and desorb without dissociation.

The adsorbed phase of N molecules (k-mers, S-mers, or k^2-mers) at temperature T and chemical potential μ can be described introducing the occupation variable c_i, where $c_i = 0, 1$ if the adsorption site is empty or occupied respectively. In this way the system of k-mers adsorbed on square and triangular lattices and the system of S-mers adsorbed on square lattices, share the same Hamiltonian,

$$H = \sum_{\langle i,j \rangle} w c_i c_j - N(k-1)w - \mu N + \varepsilon_0 \sum_i c_i, \qquad (37)$$

where w, measured in $k_B T$ units (k_B is the Boltzmann constant), represents the nearest-neighbor interaction energy and, in this work, it is considered attractive (negative). In addition ε_0 is the adsorption energy, also measured in $k_B T$ units. In the simulations, ε_0 is set equal to zero without losing generality given the surface homogeneity. The summation over $\langle i, j \rangle$ represents a summation over all pairs of nearest-neighbor sites. Finally, the second term $N(k-1)$ corrects the energy counted in excess by the first term, since it overestimates the number of first neighbors including the links belonging to the same k-mer.

On the other hand, for k^2-mers adsorbed on square lattices the Hamiltonian is given by

$$H = \sum_{\langle i,j \rangle} w c_i c_j - N2k(k-1)w - \mu N + \varepsilon_0 \sum_i c_i. \qquad (38)$$

In this case, the summation over all pairs of nearest neighbor sites overestimates the total energy by including $2k(k-1)$ internal bonds of the N adsorbed k^2-mers.

B. Monte Carlo simulations in the grand canonical ensemble

The equilibrium properties of the systems studied were obtained via Monte Carlo simulations in the grand canonical ensemble. We have used a typical parallel tempering [47–49] adsorption-desorption algorithm that generates a set of N_{rep}

different replicas of the systems, allowing to parallelize the computational calculations to reach equilibrium more efficiently. Each replica of the system is run at a different value of chemical potential and every certain number of simulation steps the configurations of two neighboring replicas are swapped. The general outline of the algorithm is described at next:

(1) An initial configuration is randomly generated for each replica.

(2) One of the N_{rep} replicas of the system is randomly selected.

(3) A linear k-uple (a set of k consecutive lattice sites) is chosen at random in that replica.

(4) If the k-uple is empty(occupied) an adsorbate is adsorbed(desorbed) with probability $P = \min\{1, \exp(-\Delta H/k_B T)\}$ where ΔH is the difference between the Hamiltonians of the initial and final states.

(5) After repeating $M = L \times L$ steps of the previous item, the configurations of two adjacent replicas are swapped with probability $P = \min\{1, \exp(-\Delta N \Delta\mu)\}$, where ΔN is the difference in the number of molecules and $\Delta\mu$ is the difference in chemical potential between the two replicas.

We define a Monte Carlo step (MCs) as $M = L \times L$ adsorption/desorption attempts per each replica, then $MCs = L \times L \times N_{\text{rep}}$. The simulations were run typically with 2×10^6 MCs, the first 1×10^6 steps were sufficient to reach equilibrium and the next 1×10^6 steps were used to compute averages. The quantities measured in the simulations were the surface coverage θ and the energy per site u, obtained as time averages over the simulation,

$$\theta = \frac{1}{M} \sum_{i}^{M} \langle c_i \rangle \tag{39}$$

and

$$u = \frac{1}{M} \langle H \rangle. \tag{40}$$

The Binder cumulant U_L of the order parameter $m = \theta - \langle\theta\rangle$ is obtained using the histogram reweighting (HR) technique [40–42], in the same way as in our previous works [44,45], hence two-dimensional histograms $W(H, N)$ were constructed throughout the simulation to apply this methodology.

C. Monte Carlo simulation results

As it was mentioned at the beginning of this section, four different systems were studied by means of Monte Carlo simulations: linear k-mers on square lattices, linear k-mers on triangular lattices, k^2-mers on square lattices, and S-mers on square lattices.

The results obtained for the different systems regarding the adsorption isotherms are shown in Fig. 5. In all cases, the adsorption isotherms shift to lower values of chemical potential, and their slopes increase as the interaction energy w increases (in absolute value). These results are in accordance with the known fact that higher attractive interactions favours the adsorption. The results in Fig. 5 also show that, for interactions above certain critical interaction energy w_c, the isotherms of all systems exhibit a marked discontinuity

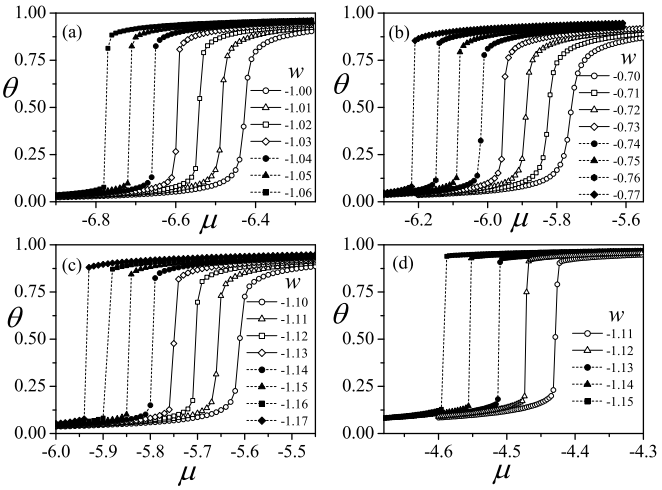

FIG. 5. Adsorption isotherms for the different systems under study with several values of the interaction energy w. (a) corresponds to a system of linear k-mers on a square lattice with $k = 5$ and $M = 100 \times 100$. In (b) we have a system of linear k-mers with $k = 3$ (trimers) adsorbed on a triangular lattice of size 120×120. A system of S-mers of size $k = 4$ on a square lattice with $L = 80$ is shown in (c) and, finally, in (d) it can be seen the isotherms corresponding to a system of k^2-mers of size 2×2 adsorbed on a square lattice of $M = 80 \times 80$ lattice sites.

between the diluted or "lattice-gas" phase at low coverage and the condensed or "liquid" phase at higher coverages. This behavior evidence that all the systems studied here, experiences a condensation-evaporation phase transition.

Therefore, it is expected that the density (or surface coverage) distribution function of these systems exhibit the features mentioned in Sec. II, resulting in the maximum of the Binder cumulant and the isotherm inflection point occurring at the same value of chemical potential. To validate the previous statement we have constructed the distribution functions from the two-dimensional histograms $W(H, N)$ obtained from the simulations and the results are shown in Fig. 6. As it can

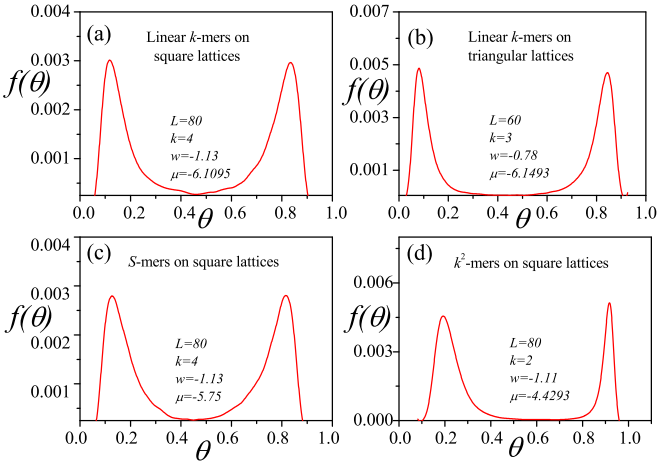

FIG. 6. Density or surface coverage distribution function for the four systems studied. The type of system for which every distribution correspond as well as the simulation parameters are indicated in each graph.

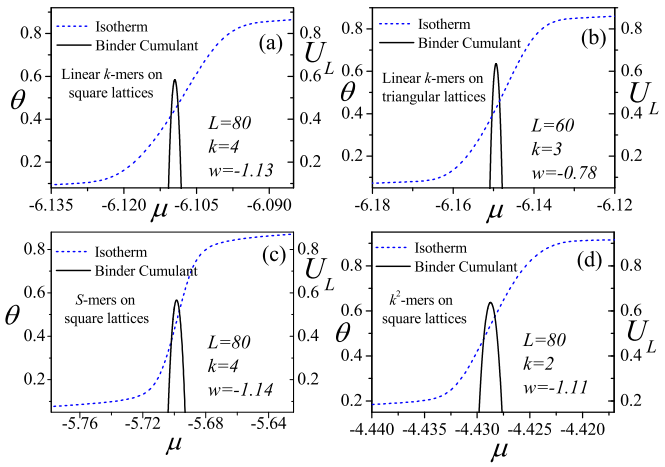

FIG. 7. Binder cumulant of the order parameter $m = \theta - \langle\theta\rangle$ plotted as a function of μ along with the adsorption isotherm for the different systems under study. The symbology, the simulation parameters and to which system corresponds each curve are indicated in the graph. In all cases the maximum of the Binder cumulant coincides with the isotherm inflection point.

be seen, all the lattice coverage distribution functions obtained here exhibit a bimodal behavior consistent with typical condensation-evaporation systems distributions. In addition, the two peaks representing the two phases (diluted and condensed) resemble two Gaussian-like curves. It is worth remembering that the hypotheses formulated in Sec. II do not impose any particular form for the distribution function (the only requirement is that it be a bimodal curve).

In Fig. 7 the Binder cumulant of the different systems is plotted, as a function of the chemical potential, along with the adsorption isotherm. As it was expected from the analysis of the distribution functions, it can be seen that for all the systems studied in the present work, the maximum of the Binder cumulant and the isotherm inflection point take place at the same value of chemical potential. In the four graphs the same behavior is observed, the variability of the cumulant is contained in a very small range of chemical potential which produces that its maximum is well located over the inflection point of the isotherm.

IV. SUMMARY AND CONCLUSIONS

In the present article the study of evaporation-condensation systems was addressed to present arguments that explain the crucial observation in the development and application of the maximum cumulant method, that is, the maximum of the Binder cumulant and the inflection point of the isotherm occurring at the same value of chemical potential. In this sense, we have presented mathematical arguments that show how, under certain general conditions this observation can be explained for this type of systems.

From this mathematical formulation we were able to show that the maximum cumulant method is valid for any evaporation-condensation system whose density distribution function exhibits certain general characteristics. In particular, this must be a bimodal function where the distributions representing the two phases do not necessarily have to be of the same type, nor have a particular form such as Gaussian (as has been assumed in many approaches), but it is sufficient to require that they be symmetrical with respect to the middle point.

In addition, we have conducted MC simulations on different condensation-evaporation systems to test the general validity of the maximum cumulant method. The results show that, in all the cases studied, the maximum of the Binder cumulant curve and the isotherm inflection point are found for the same value of chemical potential, making the MCM applicable. The case of the system of adsorption of square tiles is especial, since it shows that in despite of having a density distribution with asymmetric peaks, the maximum of the cumulant and the inflection point still coincide at the same value of μ. This suggests that the applicability of the method covers even more systems than those dictated by the hypotheses formulated in Sec. II, which allowed to obtain, in an analytical manner, a corroboration of this method. This robustness shown by the method merits further research aimed at obtaining a corroboration from the formulation of more general hypotheses (this investigations are currently being carried out by the authors).

ACKNOWLEDGMENTS

This work was supported in part by CONICET (Argentina) under Project No. PIP 112-201101-00615; Universidad Nacional de San Luis (Argentina) under Projects No. 03-0816 and No. 03-2516; and the National Agency of Scientific and Technological Promotion (Argentina) under Project No. PICT-2013-1678. The numerical work were done using the BACO parallel cluster (composed by 70 PCs each with an Intel i7-3370 / 2600 processor) located at Instituto de Física Aplicada, Universidad Nacional de San Luis-CONICET, San Luis, Argentina.

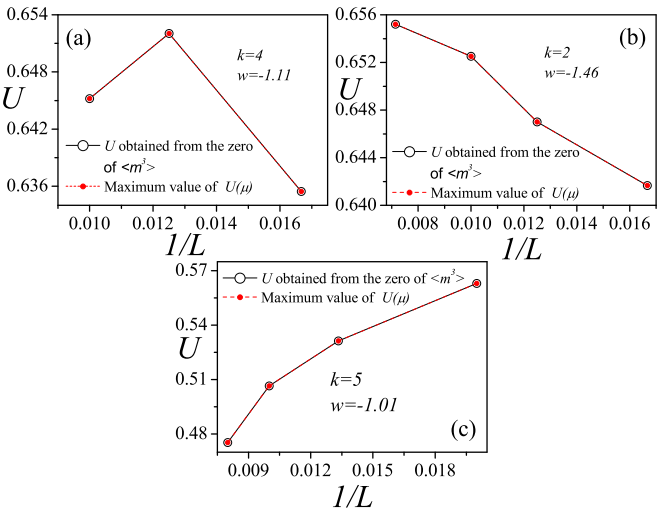

FIG. 8. Comparison between the two approaches. The different graphs correspond to square tiles or k^2-mers of size $k = 2$ (a), dimers $k = 2$ (b), and pentamers $k = 5$ (c) all adsorbed on square lattices of different sizes.

APPENDIX

The mean value of the lattice coverage can be obtained from the partition function as

$$\langle\theta\rangle = \frac{1}{N_{\max}} \frac{\sum N\, e^{(-\beta U_N + \beta\mu N)}}{\sum e^{(-\beta U_N + \beta\mu N)}}, \tag{A1}$$

where U_N is the total energy of the system with N particles and $\beta = 1/k_B T$ as usual. In addition, the Binder cumulant can be written as

$$U = \frac{-1}{(\beta N_{\max})^3 3\langle m^2\rangle^2} \frac{\partial^3\langle\theta\rangle}{\partial\mu^3}. \tag{A2}$$

That is, the expression for the Binder cumulant is a product of functions that depend on μ. Thus, differentiating to find the location of the maximum, the following expression is obtained:

$$\frac{\partial U}{\partial\mu} = \frac{-1}{(\beta N_{\max})^3}\left[\frac{\partial^4\langle\theta\rangle/\partial\mu^4}{3\langle m^2\rangle^2} - \frac{\partial^3\langle\theta\rangle}{\partial\mu^3}\left(\frac{1}{(3\langle m^2\rangle^2)^2}\right)6\langle m^2\rangle\frac{\partial\langle m^2\rangle}{\partial\mu}\right]. \tag{A3}$$

Given that $\frac{\partial\langle m^2\rangle}{\partial\mu} = \frac{\partial^2\langle\theta\rangle}{\partial\mu^2}\frac{1}{(\beta N_{\max})} = (\beta N_{\max})\langle m^3\rangle$, if the distribution $f(\theta)$ is symmetric, then $\langle m^3\rangle = \langle m^5\rangle = 0$ at certain μ and the cumulant has its maximum at this value of μ, too.

If this is not the case, one could determine the chemical potential of the inflection point using the maximum of the second moment or zero of the third moment, and then calculate the Binder cumulant. We have performed calculations with this method to compare this result with the ones obtained by the MCM. In Fig. 8, we show a comparison of the cumulant values obtained from the two methodologies. It can be seen that for all the cases studied there is no difference between the two approaches mentioned in the text, even for small systems. We can confirm that both methods coincide in the determination of the value of the cumulant up to the fourth or even the fifth significant digit.

[1] H. E. Stanley, *Introduction to Phase Transitions and Critical Phenomena* (Oxford University Press, Oxford, 1987).
[2] M. Plischke and B. Bergersen, *Equilibrium Statistical Physics* (World Scientific, Singapore, 2006).
[3] N. Goldenfeld, *Lectures on Phase Transitions and the Renormalization Group*, Advanced Book Program (Addison-Wesley, Reading, MA, 1992).
[4] J. M. Yeomans, *Statistical Mechanics of Phase Transitions* (Clarendon Press, London, 1992).
[5] S. Puri and V. Wadhawan, *Kinetics of Phase Transitions* (CRC Press, Boca Raton, FL, 2009).
[6] E. Ising, Z. Physik **31**, 253 (1925).
[7] T. L. Hill, *An Introduction to Statistical Thermodynamics* (Addison Wesley, Reading, MA, 1960).
[8] C. Domb, in *Phase Transitions and Critical Phenomena*, edited by C. Domb and M. S. Green (Academic Press, London, 1974), Vol. 3, p. 1.
[9] M. E. Fisher, Rep. Prog. Phys. **30**, 615 (1967).
[10] L. Onsager, Phys. Rev. **65**, 117 (1944).
[11] M. J. Hostetler, W. L. Manner, R. G. Nuzzo, and G. S. Girolami, J. Phys. Chem. **99**, 15269 (1995).
[12] J. J. Potoff and J. I. Siepmann, Phys. Rev. Lett. **85**, 3460 (2000).
[13] J. J. Potoff and J. I. Siepmann, Langmuir **18**, 6088 (2002).
[14] P. Zeppenfeld, J. Goerge, V. Diercks, R. Halmer, R. David, G. Comsa, A. Marmier, C. Ramseyer, and C. Girardet, Phys. Rev. Lett. **78**, 1504 (1997).
[15] O. G. Mouritsen and A. J. Berlinsky, Phys. Rev. Lett. **48**, 181 (1982).
[16] D. Ferry and J. Suzanne, Surf. Sci. **345**, L19 (1996).
[17] J. W. He, C. A. Estrada, J. S. Corneille, M. C. Wu, and D. W. Goodman, Surf. Sci. **261**, 164 (1992).
[18] V. Panella, J. Suzanne, P. N. M. Hoang, and C. Girardet, J. Phys. I. France **4**, 905 (1994).
[19] D. L. Meixner, D. A. Arthur, and S. M. George, Surf. Sci. **261**, 141 (1992).
[20] K. Binder, *Applications of the Monte Carlo Method in Statistical Physics: Topics in Current Physics* (Springer, Berlin, 1984), Vol. 36.
[21] K. Binder and D. P. Landau, Phys. Rev. B **21**, 1941 (1980).
[22] D. P. Landau, Phys. Rev. B **27**, 5604 (1983).
[23] K. Binder and D. P. Landau, Phys. Rev. B **30**, 1477 (1984).
[24] D. P. Landau and K. Binder, Phys. Rev. B **31**, 5946 (1985).
[25] D. P. Landau and K. Binder, Phys. Rev. B **41**, 4633 (1990).
[26] M. Borówko and W. Rżysko, J. Colloid Interface Sci. **244**, 1 (2001).
[27] W. Rżysko and M. Borówko, J. Chem. Phys. **117**, 4526 (2002).
[28] W. Rżysko and M. Borówko, Surf. Sci. **520**, 151 (2002).
[29] W. Rżysko and M. Borówko, Surf. Sci. **600**, 890 (2006).
[30] W. Rżysko and M. Borówko, Phys. Rev. B **67**, 045403 (2003).
[31] A. J. Ramirez-Pastor, J. L. Riccardo, and V. D. Pereyra, Surf. Sci. **411**, 294 (1998).
[32] F. Romá, A. J. Ramirez-Pastor, and J. L. Riccardo, Phys. Rev. B **68**, 205407 (2003).
[33] F. Romá, A. J. Ramirez-Pastor, and J. L. Riccardo, Phys. Rev. B **72**, 035444 (2005).
[34] P. M. Pasinetti, F. Romá, J. L. Riccardo, and A. J. Ramirez-Pastor, Phys. Rev. B **74**, 155418 (2006).
[35] F. Romá, J. L. Riccardo, and A. J. Ramirez-Pastor, Phys. Rev. B **77**, 195401 (2008).
[36] A. J. Ramirez-Pastor, J. L. Riccardo, and V. D. Pereyra, Langmuir **16**, 10167 (2000).
[37] J. E. González, A. J. Ramirez-Pastor, and V. D. Pereyra, Langmuir **17**, 6974 (2001).
[38] A. Patrykiejew, S. Sokolowski, and K. Binder, Surf. Sci. Rep. **37**, 207 (2000).

[39] M. S. Nazzarro, A. J. Ramirez-Pastor, J. L. Riccardo, and V. D. Pereyra, Surf. Sci. **391**, 267 (1997).
[40] A. Z. Panagiotopoulos, J. Phys.: Condens. Matter **12**, R25 (2000).
[41] A. M. Ferrenberg and R. H. Swendsen, Phys. Rev. Lett. **61**, 2635 (1988).
[42] A. M. Ferrenberg and R. H. Swendsen, Phys. Rev. Lett. **63**, 1195 (1989).
[43] H. Müller-Krumbhaar and K. Binder, *Monte Carlo Methods in Statistical Physics*, Topics in Current Physics (Springer-Verlag, Berlin, Heidelberg, 1979).
[44] G. J. dos Santos, D. H. Linares, and A. J. Ramirez-Pastor, J. Stat. Mech. (2017) 073211.
[45] G. J. dos Santos, D. H. Linares, and A. J. Ramirez-Pastor, Physica A **495**, 81 (2018).
[46] T. L. Hill, *Thermodynamics of Small Systems* (Dover, New York, 1962).
[47] R. H. Swendsen and J.-S. Wang, Phys. Rev. Lett. **57**, 2607 (1986).
[48] D. J. Earl and M. W. Deem, Phys. Chem. Chem. Phys. **7**, 3910 (2005).
[49] K. Hukushima and K. Nemoto, J. Phys. Soc. Jpn. **65**, 1604 (1996).